Time Response Stress Analysis of Solid and Reinforced Thin-Walled Structures by Component-Wise Models

# Time response stress analysis of solid and reinforced thin-walled structures by component-wise models

R. Azzara*, E. Carrera†, M. Filippi‡, A. Pagani§

*Mul*$^2$ group

Department of Mechanical and Aerospace Engineering, Politecnico di Torino

Corso Duca degli Abruzzi 24, 10129 Torino, Italy

**Abstract:** *This paper deals with the evaluation of time response analyses of typical aerospace metallic structures. Attention is focussed on detailed stress state distributions over the time, so the Carrera Unified Formulation (CUF) is used for modelling thin-walled reinforced shell structures. In detail, the already established component-wise (CW) approach is extended to dynamic time response by mode superposition and Newmark direct integration scheme. CW is a CUF-based modelling technique which allows to model multi-component structures by using the same refined finite element for each structural component, e.g., stringers, panels, ribs. Components coupling is realized by imposing displacement continuity without the need of mathematical artifices in the CW approach, so the stress state is consistent in the entire structural domain. The numerical results discussed include thin-walled open and closed section beams, wing boxes and a benchmark wing subjected to gust loading. They show that the proposed modelling technique is effective. In particular, as CW provides reach modal bases, mode superposition can be significantly efficient, even in the case of complex stress states.*

**Keywords:** Dynamic response; Carrera Unified Formulation; Newmark method; Mode superposition method; Stress analysis.

*PhD student. E-mail: rodolfo.azzara@polito.it

†Professor of Aerospace Structures and Aeroelasticity. E-mail: erasmo.carrera@polito.it

‡Assistant professor. E-mail: matteo.filippi@polito.it

§Associate professor. E-mail: alfonso.pagani@polito.it

# 1 Introduction

The study of the dynamic behaviour of structures is a crucial point for the design of various structural components. In particular, in aerospace engineering applications, as reported by Hernandez *et al.* [1], performing an accurate dynamic analysis is essential in the design of aircraft to understand the structural behaviour of the structure when subject to conditions of time-varying loads. As mentioned by Carrera *et al.* [2], to carry out analyses of fatigue, failure effects and aeroelastic instability, it is necessary to know the dynamic properties of the structural component of the aircraft correctly. The dynamic response of structures continues to receive the attention of many researchers and scientists. For instance, Beskos and Leung [3] proposed a method based on the combination of the finite element (FE) method, Laplace formulation and finite difference method for analyzing the dynamic response in plate structures. In the framework of geometrical nonlinearity, the dynamic response of anisotropic sandwich structures was conducted by Librescu *et al.* [4] for investigating the effect of the core, material properties and structural damping. Parhi *et al.* [5] used an eigh-noded isoparametric quadratic element to implement a procedure to perform dynamic response of delaminated composite plate structures. Geometrical and constitutive non-linearities were considered by Mata *et al.* [6] to describe the dynamic analysis of beam structures, including the viscosity. In [7], the authors presented the dynamic analysis of inflated beam aerospace structures to investigate the damping and to develop an accurate procedure to analyze complex structures. In recent years, different types of slender structures are increasingly used in aerospace, such as in rockets, launchers, fuselage and aircraft wings. Many researchers have addressed their studies on the modelling of these structures. These structures can be modelled through one-dimensional (1D) models. One of the main advantages of the 1D model is the lower computational cost required compared to two-dimensional (2D) formulations. In the last decades, much effort was made to improve and refine the classical beam theories, the Euler-Bernoulli Beam Theory (EBBT) [8] and the Timoshenko Beam Theory (TBT) [9, 10], in order to overcome their assumptions. These improvements aimed to include shear correction factors [11], rotary inertia [12] and warping effects [13]. Readers are referred to [14] for a comprehensive and detailed review of modern beam models.

Recently, refined theories in the framework of the 1D Carrera Unified Formulation (CUF) [15] have shown significant advances in dynamic analysis. CUF represents a hierarchical formulation in which the order of the structural model is considered input of the analysis. CUF was implemented first for plates and shells [16, 17] and, subsequently, also for beams [18, 19]. As an example, Carrera

and Varello [20] provided the dynamic analysis of thin-walled structures using the Taylor-expansion (TE). In contrast, in [21] the cross-sectional kinematics of 1D models is approximated by Lagrange Expansion (LE) polynomials.

In this paper, dynamic analyses of the structures of aerospace relevance are discussed by combining CUF beam theories with different dynamic formulations, such as the Newmark method [22] and the mode superposition method [22, 23], which are widely used in structural dynamics. In the open literature, there are many articles that use these methods. For instance, Chaudhary and Bathe [24] performed the time integration of the dynamic response of a three-dimensional contact problem with friction using the Newmark method. Borino and Muscolino [25] presented a new method based on the mode superposition method and the dynamic correction method to evaluate the dynamic response of damped linear structures. A procedure based on the combination of the mode superposition method and the pseudo-force theory for performing dynamic response of structures considering non-proportional damping was implemented by Claret and Venancio-Filho [26]. Hansteen and Bell [27] presented an accurate mode superposition technique for performing analysis in structural dynamics. Ma and Hagiwara [28] introduced an innovative mode superposition formulation adopting the orthogonality condition to obtain the modal frequency response of coupled acoustic-structural models. Pagani *et al.* [29] described the dynamic analysis of aerospace structures adopting the mode superposition method.

One of the main advantages of the mode superposition method is that the system of equations is written in modal coordinates and eventually decoupled. As reported by Ma and Hagiwara [28], the number of modes to be used in the mode superposition method to perform dynamic analyses of a structure is typically smaller than the total number of variables of the FE model. It is important to emphasize that employing a standard mode superposition technique (mode displacement method), few modes are necessary to accurately evaluate displacements, while stress distributions are inaccurate [30]. To correct these inaccuracies, the mode acceleration method [31] is employed in structural dynamics and, in particular, for stress assessment.

This article presents the dynamic analysis of a number of aeronautical structures subjected to time-dependent loadings to evaluate both displacements and stress distributions. First, displacements using both the Newmark method and mode superposition method are obtained; then, a three-dimensional (3D) stress distributions are reported. The 3D nature of CUF allows the prediction of the stresses with a level of accuracy that depends on the selected theory order. Convergence analyses demonstrate how a different number of modes are needed for the correct assessment of

displacements and stresses through the mode superposition method. Moreover, this work focuses particular attention on the use of the component-wise (CW) method. In the domain of the CW methodology, each component of the structure can be approximated independently via 1D models with higher-order approximation. It is generally accepted that primary aircraft structures are reinforced thin shells [32]. As a matter of fact, in the present study, we used the component-wise approach to model reinforced-shell aircraft structures. For these structures, the determination of stress distributions is fundamental. Many works on the CW approach can be found in the literature [33, 34, 35, 36].

The present manuscript is structured as follows: (i) first, Section 2 introduces CUF, with particular emphasis on CW approach, and dynamic formulations used; (ii) then, Section 3 discusses the numerical results; (iii) finally, Section 4 reports the conclusions.

## 2 Carrera Unified Formulation

### 2.1 Preliminaries

Figure 1 shows a typical reinforced structure in a Cartesian reference system. The displacement vector is introduced as:

$$\boldsymbol{u}(x,y,z;t) = \{u_x \; u_y \; u_z\}^T \tag{1}$$

The stress and strain components ($\boldsymbol{\sigma}$ and $\boldsymbol{\epsilon}$ respectively) are written in vectorial form as:

$$\begin{aligned} \boldsymbol{\sigma} &= \{\sigma_{xx} \; \sigma_{yy} \; \sigma_{zz} \; \sigma_{xz} \; \sigma_{yz} \; \sigma_{xy}\}^T \\ \boldsymbol{\epsilon} &= \{\epsilon_{xx} \; \epsilon_{yy} \; \epsilon_{zz} \; \epsilon_{xz} \; \epsilon_{yz} \; \epsilon_{xz}\}^T \end{aligned} \tag{2}$$

Considering the case of small displacements, linear strain displacements relations are used. It reads:

$$\boldsymbol{\epsilon} = \boldsymbol{D}u \tag{3}$$

where $\boldsymbol{D}$ represents a linear differential operator. The stresses are computed from the constitutive relations:

$$\boldsymbol{\sigma} = \boldsymbol{C}\epsilon \tag{4}$$

Details are not provided here; readers are referred to [15].

According to 1D CUF, the displacement field $\boldsymbol{u}(x,y,z;t)$ is an expansion of generic functions

$F_\tau$(x,z) for the generalized displacements vector $\boldsymbol{u_\tau}(y;t)$. Hence:

$$\boldsymbol{u}(x,y,z;t) = F_\tau(x,z)\ \boldsymbol{u}_\tau(y;t) \qquad \tau = 1,2,...,M \tag{5}$$

where $M$ represents the number of terms of the expansion and $\tau$ indicates summation. The selection of $F_\tau$ determines the class of the 1D CUF models. CUF may employ both Lagrange expansions (LE) and Taylor expansions (TE) in static and dynamic analyses. As observed in the literature, TE may be adequate for describing the global response (transverse deflection), instead, LE is preferred to accurately capture the complete 3D stress field. For a detailed review of different displacement fields, readers are referred to [21]. Note that it is recognized that refined formulations are necessary when beam structures are short, thin-walled, or with open cross-section.

## 2.2 Component-Wise approach via CUF

The component-wise (CW) method was introduced in the domain of CUF in recent works [33, 35, 36]. According to the CW approach, each component is modelled through the 1D CUF-based finite elements. The CW approach favours the advancements of the model capabilities by (1) choosing which component requires a more detailed model; (2) setting the order of the structural model to be adopted. In this paper, the LE formulation was assumed to implement CW models to divide the cross-section into various sub-domains, for instance, stringers and panels, see Fig 1. Each single LE

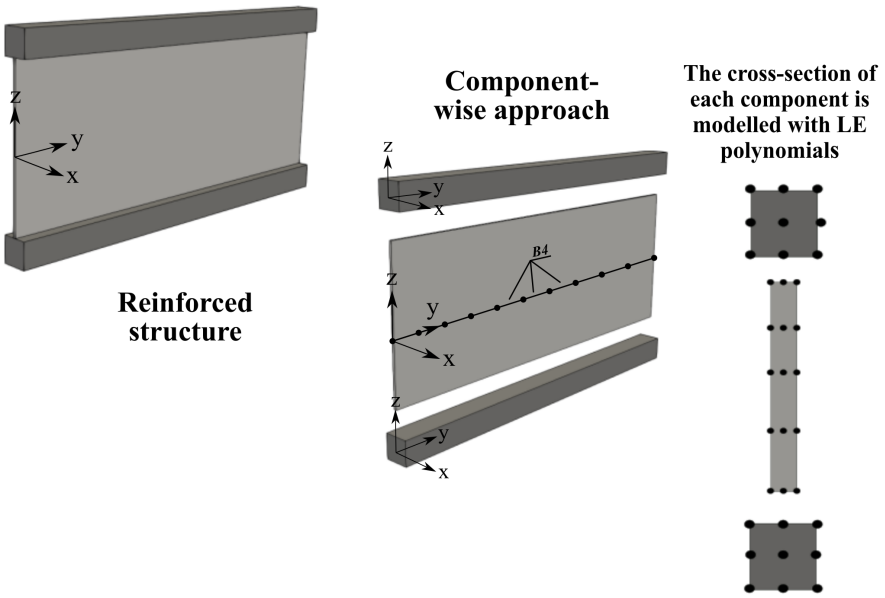


Figure 1: Component-wise approach to model panel and stringers.

element, maintaining its geometric and material characteristics, is, then, assembled to compute the

global stiffness matrix.

When using LE in a CW scenario, the cross-section of the structure is interpreted as the sum of different sub-domains, in which the discretization is made using refined 1D CUF models. LE is of particular interest because they use only displacement unknowns. This allows us to impose displacement continuity among components in a natural manner and without using mathematical artifices. This is not the case of TE, which was extended to multi-component structures by Carrera and Pagani [37, 38]. In this case, continuity was imposed by Lagrange multipliers. As a consequence, ghost forces were present with repercussions on stress state close to coupling zones.

### 2.3 Finite Element Formulation

In this article, the equations of motion are approximated using the finite element method (FEM) and solved with direct integration scheme and mode superposition. According to FEM, the generalized displacement vector $\mathbf{u}_\tau$ is interpolated along the $y$-direction using the shape functions $N_i$:

$$\mathbf{u}(x, y, z; t) = F_\tau(x, z) N_i(y) \mathbf{q}_{\tau i}(t) \tag{6}$$

where $\mathbf{q}_{\tau i}$ contains the degrees of freedom of the $\tau^{th}$ expansion term corresponding to the i$^{th}$ element node. If not differently stated, we make use of four-node cubic beam elements (B4) in this work as shape functions. The selection of the cross-section discretization for the CW class or the theory order, N, for the TE class is completely arbitrary. Readers are referred to [39] for further details.

Stiffness and mass matrices of the elements are formulated using the principle of virtual displacements.

$$\delta L_{int} = \int_V \delta \boldsymbol{\epsilon}^T \boldsymbol{\sigma} dV = \delta L_{ext} - \delta L_{ine} \tag{7}$$

where $\delta L_{int}$, $\delta L_{ext}$ and $\delta L_{ine}$ represent the virtual variation of the strain energy, external loadings and inertial loads, respectively. In this paper, structural damping is not considered. The expression of the internal strain energy can be written in terms of virtual nodal displacements as follows:

$$\delta L_{int} = \delta \mathbf{q}_{\tau i}^T \mathbf{K}^{ij\tau s} \mathbf{q}_{sj} \tag{8}$$

where $\mathbf{K}^{ij\tau s}$ represents the fundamental nucleus of the stiffness matrix and the superscripts denote the four indexes exploited to expand the element matrix. Readers are referred to [15] for the complete derivation of this matrix. The virtual variation of the work of inertial loading is formulated in the

following compact notation:

$$\delta L_{ine} = \delta \mathbf{q}_{\tau i}^{T} \mathbf{M}^{ij\tau s} \ddot{\mathbf{q}}_{sj} \tag{9}$$

where $\mathbf{M}^{ij\tau s}$ is the fundamental nucleus of the mass matrix and double dot denotes double derivative with respect to time. Similarly, the virtual work of an external point load $\mathbf{F}$ is:

$$\delta L_{ext} = \delta \mathbf{q}_{\tau i}^{T} \mathbf{F}_{\tau i} \tag{10}$$

Finally, the undamped dynamic problem can be formulated as following:

$$\mathbf{M}\ddot{\mathbf{q}}(t) + \mathbf{K}\mathbf{q}(t) = \mathbf{F}(t) \tag{11}$$

### 2.3.1 Newmark method

Equation 11 is a system of algebraic equations in the time domain. The resolution may involve the use of a time integration scheme, such as the Newmark method. This method, largely adopted in structural dynamics, belongs to the family of direct integration methods [22]. For the sake of completeness, the equation of motion at time t+Δt and its solution is reported here.

$$\mathbf{M}\ddot{\mathbf{q}}_{t+\Delta t} + \mathbf{K}\mathbf{q}_{t+\Delta t} = \mathbf{F}_{t+\Delta t} \tag{12}$$

The step-by-step solution of Eq. (12) is obtained using the following assumptions for the velocities and displacements within the time step Δt:

$$\begin{aligned} \dot{\mathbf{q}}_{t+\Delta t} &= \dot{\mathbf{q}}_t + [(1-\delta)\ddot{\mathbf{q}}_t + \delta\ddot{\mathbf{q}}_{t+\Delta t}]\Delta t \\ \mathbf{q}_{t+\Delta t} &= \mathbf{q}_t + \dot{\mathbf{q}}_t\Delta t + [(\tfrac{1}{2}-\alpha)\ddot{\mathbf{q}}_t + \alpha\ddot{\mathbf{q}}_{t+\Delta t}]\Delta t^2 \end{aligned} \tag{13}$$

where $\alpha$ and $\delta$ represent parameters that are determined to obtain integration accuracy stability. In this paper, $\delta$= 0.5 and $\alpha$= 0.25 are considered for the related constants [22]. Considering the trapezoidal rule, $\dot{\mathbf{q}}_{t+\Delta t}$ and $\ddot{\mathbf{q}}_{t+\Delta t}$ are computed from Eq. (13) in terms of $\mathbf{q}_{t+\Delta t}$. Then, we solve for each time step:

$$\widehat{\mathbf{K}}\mathbf{q}_{t+\Delta t} = \widehat{\mathbf{F}}_{t+\Delta t} \tag{14}$$

where:

$$\widehat{\mathbf{K}} = \mathbf{K} + \frac{1}{\alpha(\Delta t)^2}\mathbf{M} \tag{15}$$

$$\widehat{\mathbf{F}} = \mathbf{F} + \frac{1}{\alpha(\Delta t)}\mathbf{M}\dot{\mathbf{q}}_t + \frac{1}{2\alpha}\mathbf{M}\ddot{\mathbf{q}}_t \tag{16}$$

This procedure is repeated for all the time steps. The complete solution procedure using the Newmark method is given in [22].

### 2.3.2 Mode superposition method

Thanks to the accuracy of the modal analyses performed with the CUF, the mode superposition method turns out to be very advantageous in dynamic analyses when the Newmark method is too computationally expensive. The undamped dynamic force equilibrium is reported in Eq. (11). It can be expressed in the modal coordinates by using the following transformation:

$$\mathbf{q}(t) = \mathbf{\Phi}\mathbf{x}(t) \tag{17}$$

where $\mathbf{\Phi}$ represents a *DOFs* x $m$ matrix containing $m$ $\boldsymbol{M}$-orthonormalized eigenvectors and $\mathbf{x}(t)$ indicates a time-dependent vector of order $m$. If damping neglected, the equilibrium equations become:

$$\ddot{\mathbf{x}}(t) + \mathbf{\Omega}^2\mathbf{x}(t) = \mathbf{\Phi}^T\mathbf{F}(t) \tag{18}$$

where $\mathbf{\Omega}^2$ represents the diagonal matrix that stores the second power of the natural periods $\omega_i^2$. Equation (18) is a system of $m$ individual equations of the form:

$$\begin{cases} \ddot{x}_i(t) + \omega_i^2 x_i(t) = r_i(t) \\ r_i(t) = \mathbf{\Phi}_i^T\mathbf{F}(t) \end{cases} \tag{19}$$

The solution of each Eq. (19) is computed introducing the well-known Duhamel integral. By using this procedure, the contributions to the response for each mode is computed. Naturally, the accuracy of the solution will depend on the number $m$. All details about the various parameters are not reported here. Readers are referred to [22] for the complete description of this method.

## 3 Numerical Results

This section discusses representative numerical examples and particular emphasis is given to the capabilities of the proposed method to perform time response stress analysis. For this purpose, we investigate the effectiveness of both mode superposition and Newmark methods when coupled with

the CUF-based CW modelling approach. Note that for all the numerical experiments, damping is neglected. For the sake of completeness, for the first two cases the convergence analysis for different discretization theories on the cross-section, from lower-order to higher-order, is also reported. Results suggest that a low-order model is sufficient to evaluate the normal stress, whereas a high-order model is needed to accurately predict the transverse shear stress component. For the other cases, the through-the-thickness stress distributions of the convergent model in comparison with the linear interpolation adopted by the *FSDT-like* approximation, typically considered in commercial codes, is provided. First, a square cross-section and a thin-walled structure subjected to dynamic loads are analyzed. Then, the dynamic response analyses of reinforced structures of aeronautical interest, such as a two-stringer spar, a wing box and complete NACA wing, are discussed.

### 3.1 Solid square cross-section beam under sinusoidal loading

A simply supported square cross-section beam was analyzed as the first example, see Fig. 2. The square cross-section has the following geometrical characteristics: sides are equal to 0.1 m, span-to-height ratio $L/h$ equal to 100. The whole structures has the following material data: $E$= 69 GPa, $\nu$= 0.33 and $\rho$= 2700 $kg/m^3$. This structure is modelled by means 10 B4 finite elements along the $y$-axis and a quadratic approximation is used on the cross-section (L9). The reason for using L9 was widely discussed by Carrera and Petrolo [21].

First, free-vibration analysis is carried out, and then a comparison between the mode superposition and the Newmark methods is performed. Table 1 reports the first ten natural frequencies of the

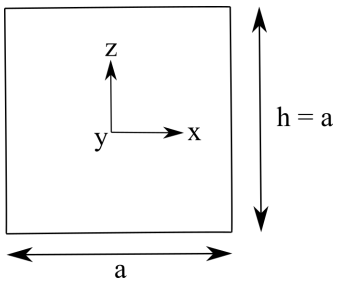


Figure 2: Compact square cross section.

structure under consideration. From this preliminary assessment, it is clear that TE 3 may be a good model for the subsequent time response analysis, as it provides good convergence. The convergence analysis by varying the number of beam elements along the $y$-axis was already performed by Carrera *et al.* [40]. For completeness reasons, some important modes of the square beam are shown in Fig. 3.

| No. mode. | Freq. TE 1 | Freq. TE 2 | Freq. TE 3 | Freq. TE 4 | Freq. L9 |
|---|---|---|---|---|---|
| 1 | 2.3895 | 2.3895 | 2.3895 | 2.3895 | 2.3895 |
| 2 | 2.3895 | 2.3895 | 2.3895 | 2.3895 | 2.3895 |
| 3 | 9.5546 | 9.5546 | 9.5540 | 9.5540 | 9.5546 |
| 4 | 9.5546 | 9.5546 | 9.5540 | 9.5540 | 9.5546 |
| 5 | 21.4887 | 21.4894 | 21.4858 | 21.4858 | 21.4892 |
| 6 | 21.4887 | 21.4894 | 21.4858 | 21.4858 | 21.4892 |
| 7 | 38.1951 | 38.1984 | 38.1868 | 38.1868 | 38.1978 |
| 8 | 38.1951 | 38.1984 | 38.1868 | 38.1868 | 38.1978 |
| 9 | 59.7051 | 59.7195 | 59.6889 | 59.6889 | 59.7180 |
| 10 | 59.7051 | 59.7195 | 59.6889 | 59.6889 | 59.7180 |

Table 1: Effect of the different expansion orders on frequency values [Hz] of the square cross section.

(a) I bending mode

(b) II bending mode

Figure 3: Bending mode shapes of the beam with square cross-section.

For the second assessment, the same compact beam is loaded with a single harmonic load applied at the center of the mid-span section:

$$P_z(t) = P_{z_0} sin(\omega t) \tag{20}$$

where $P_{z_0}$= -1000 N is the amplitude of the sinusoidal load, whereas $\omega$= 7 rad/s is the angular frequency. The dynamic response is analyzed using both the Newmark method and the mode superposition method over the time interval [0,8] s. 2000 steps ($dt$= 0.004 s) is chosen to perform direct time integration via the Newmark method. In [20], authors described the effect of the time step $dt$ on the transverse displacement. On the other hand, in the case of the mode superposition method, zero initial conditions are used and a convergence study on the number of modes to be used is necessary. Figure 4 shows the transverse displacement as function of the time in the middle of the structure for the different number of modes. It is noted that only 3 modes are sufficient for this type of analysis. The comparison between the mode superposition and the Newmark method is shown, instead, in Fig. 5. In addition, the comparison with the reference results [29] is also reported in this figure. These results confirm the validity of the two methods, which are effective when displacement response is necessary. It should be mentioned that, since only 3 modes are enough to guarantee the effectiveness of the mode superposition, for this analysis this method should be preferred because it

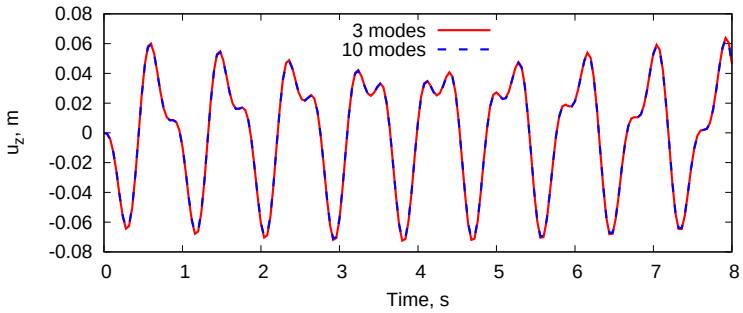


Figure 4: Convergence study of the number of modes for the mode superposition method. Square beam under sinusoidal load. TE 3 model.

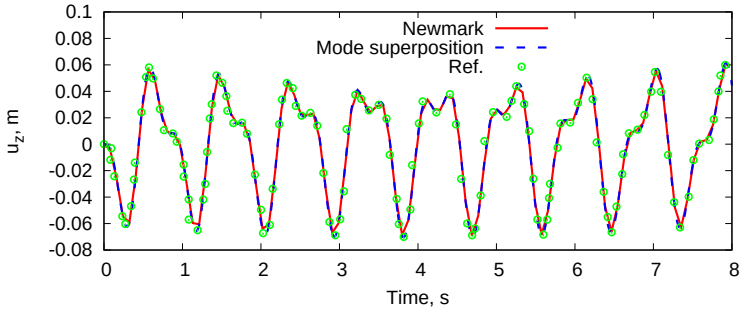


Figure 5: Transverse displacement at the mid-span section with mode superposition method (3 modes) and Newmark method ($dt$= 0.004 s, see [20]), and Ref. [29]. Square beam under sinusoidal load. TE 3 model.

is convenient in terms of computational costs. This latter aspect is shown in the subsequent analysis where this difference is even more evident.

In this work, also an evaluation of the stresses is reported. First, convergence analyses on the $dt$ and modes for the evaluation of the stresses are performed and reported in Figs. 6a and 6b. Figure 6c shows the comparison between the two methods for the shear, $\sigma_{yz}$, stress distributions as a function of the time. From Fig. 6, it can be noticed that there is a slight difference between the two resolution methods. The mode superposition allows us to evaluate stress using relatively few and correct mode shapes calculate by the proposed model. Furthermore, the resulting analyses indicate that using the mode superposition method there is a considerable time saving even for a simple model like this. This last aspect is very important to underline because it gives us a significant computational gain when dealing with more complicated structures. In addition, a comparison between the results obtained with the present method and the MSC Nastran solid model [41] results is carried out in order to provide a validation of the proposed approach. In particular, both the axial stress, $\sigma_{yy}$, and shear stress, $\sigma_{yz}$, with respect to the time are shown in Fig. 7. It should be noted that by employing the present method, it is possible to accurately derive the stress distributions

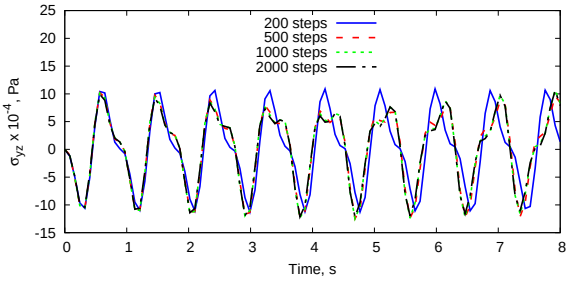


(a) Convergence analysis on the $dt$ for the Newmark method

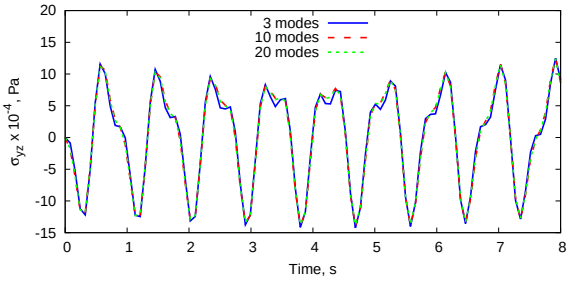


(b) Convergence analysis on the number of modes for the mode superposition method

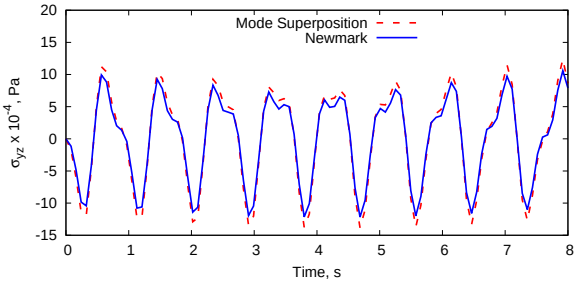


(c) Comparison between the Newmark method (500 steps) and the mode superposition method (10 modes)

Figure 6: Shear stress distributions at a quarter of the beam ($x$=$z$=0) versus time. Square beam under sinusoidal load. L16 beam model.

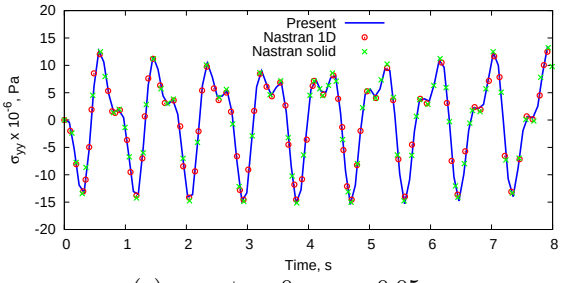


(a) $\sigma_{yy}$ at $x$=0 m, $z$= 0.05 m

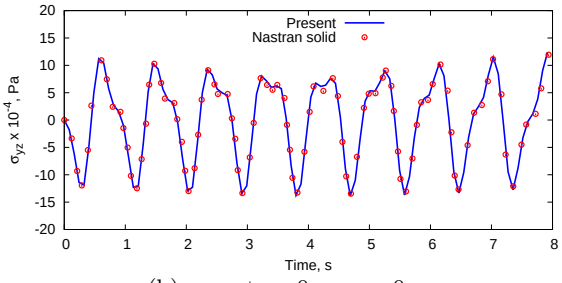


(b) $\sigma_{yz}$ at $x$=0 m, $z$= 0 m

Figure 7: Axial and shear stress distributions at a quarter of the beam versus time. Comparison between the present method and MSC Nastran solid model results. Square beam under sinusoidal load.

with a significant computational advantage than Nastran solid model due to a noticeable reduction in degrees of freedom (DOFs) (1488 vs 6102).

For the sake of completeness, the convergence analysis, see Fig. 8, for the cross-section discretization using both LE and TE theories is also reported. As a result, the cross-section of the structure was modelled with a cubic LE approximation on the cross-section (L16). Sixteen-point (L16) polynomials are considered, which lead to cubic displacement field approximations over the beam cross-section and, therefore, a better evaluation of stresses. From this figure, it is clear that a low-order model is sufficient to evaluate the normal stress $\sigma_{yy}$, whereas a high-order model is needed to accurately predict the transverse shear stress component. For example, the linear interpolation provided by the TE1 approximation is, clearly, not enough to catch the parabolic distribution of the transverse shear stress $\sigma_{yz}$. Axial and shear stress trends in the thickness direction at a quarter of the

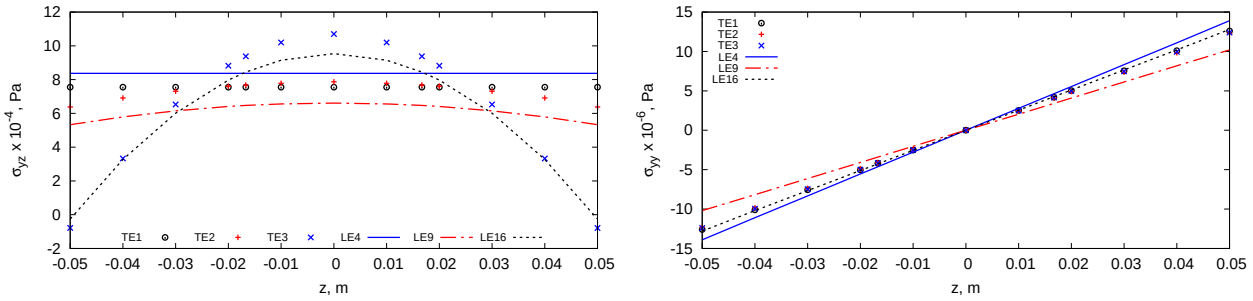


Figure 8: Through-the-thickness stress distribution at a quarter of the beam at t= 0.6 s for different LE and TE theories. Square beam under sinusoidal load.

beam, $y = L/4$, are shown in Fig. 9 at $t$= 0.6 s and $t$= 4 s using the mode superposition method. Furthermore, in these figures stress distributions adopting a theory based on linear interpolation (*FSDT-like*) is also provided, showing how inaccurate this theory is for evaluating transverse shear stress.

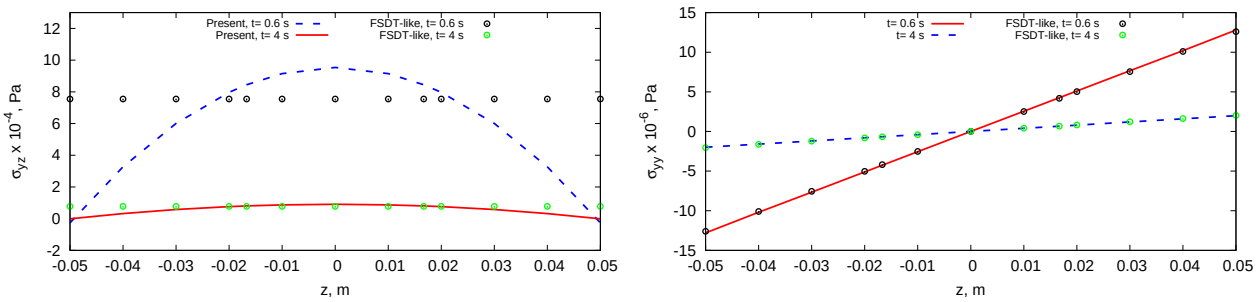


Figure 9: Through-the-thickness distribution of axial, $\sigma_{yy}$, and transverse, $\sigma_{yz}$, stress components at a quarter of the beam at different times. Square beam under sinusoidal load. Mode superposition using 10 modes. LE 16 beam model.

### 3.2 Thin-walled rectangular cross-section beam under sinusoidal loading

The dynamic response of a clamped-free beam with a thin-walled rectangular cross-section is analyzed as the second example, see Fig. 10. This model has the following geometrical data: width $a$ = 1 m, length $L$= 10 m, width-to-height ratio equal to 10, thickness $t$= 0.005 m. An isotropic material is used. The material properties are: $E$= 69 GPa, $\nu$= 0.33 and $\rho$= 2700 kg/m$^3$. As described by Carrera *et al.* [40], this structure is relatively short and will incur into cross-sectional deformations, so higher-order theories are necessary. This beam is modelled with 10 B4 finite elements along the $y$-axis and a piece-wise quadratic model on the cross-section (10L9) adopting a CW approach. A

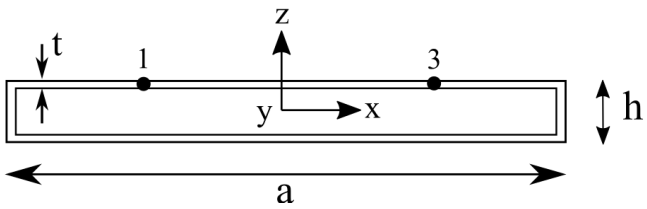


Figure 10: Thin-walled rectangular cross-section.

time-dependent sinusoidal load with amplitude $P_{z_0}$= -10000 and angular frequency $\omega$= 30 rad/s is applied at point 1 in $y = L/4$. Both the static analysis and the effect of the expansion orders on the cross-section deformation are provided by Carrera and Varello [20]. The dynamic analysis is performed over the interval [0,1.5] s. Both the Newmark method and mode superposition method are used for these dynamic analyses. A convergence study, see [20], shows that an appropriate time step in the Newmark method for this analysis is $dt$= 3×10$^{-3}$ s (500 steps). As in the previous case, a convergence study on the number of modes to use for the mode superposition method for evaluating transverse displacements is performed. The transverse displacement with respect to the time for the different number of modes and the comparison between mode superposition and Newmark method and reference results [20] at points 1 are shown in Figs. 11a and 11b, respectively. As a result, 35 modes are an appropriate choice for the evaluation of the transverse displacement. As can be noticed in these figures, the two methods show a similar trend, but also for this relatively simple structure, the mode superposition method allows us to perform a better evaluation of the displacement, in particular near the peaks.

The second part of this section presents the stress assessment. Using the mode superposition method, a new convergence analysis on the number of modes is necessary for a correct stress assessment. Figure 12 compares the shear stress versus time for the different number of modes. Overall, it can be seen that more modes should be used for the evaluation of stresses. In this case, 100

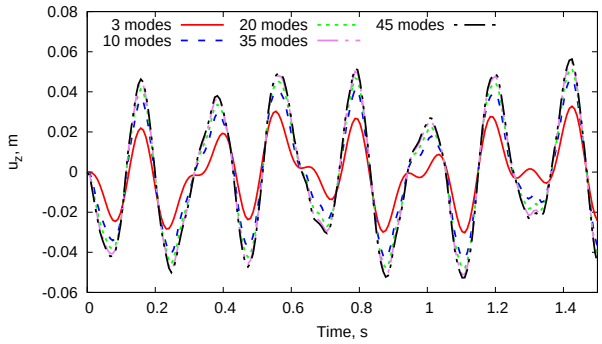


(a) Effect of the number of modes

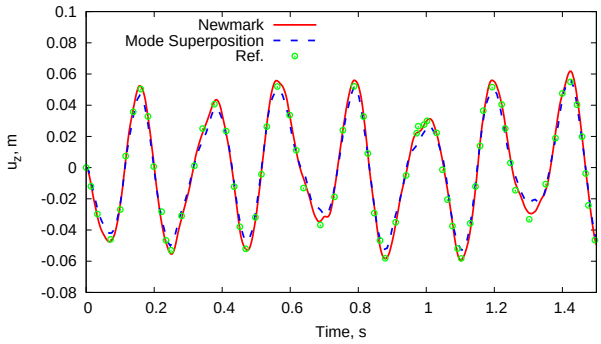


(b) Comparison between mode superposition (35 modes) and Newmark method ($dt$= 3x10$^{-3}$ s) and Ref. [20]

Figure 11: Transverse displacement of point 1 versus time. Thin-walled rectangular cross-section under sinusoidal load. L9 beam model.

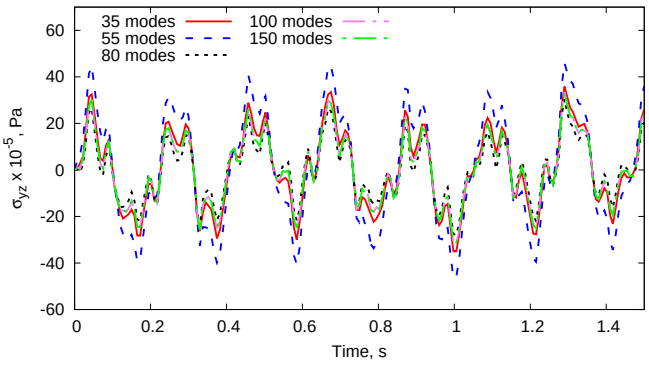


Figure 12: Convergence analysis on the number of modes for the stress evaluation. Mode superposition method. Thin-walled rectangular beam under sinusoidal load. L9 beam model.

modes are necessary to perform a correct analysis. The variation in the axial and shear stresses as a function of the time at $x$= 0.495 m and $y = L/2$ is presented in Fig. 13. As mentioned previously,

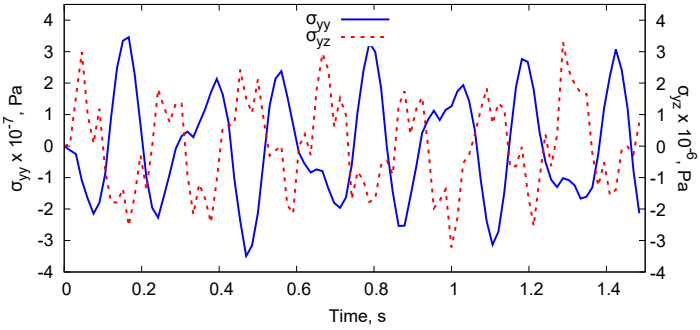


Figure 13: Axial (at $x$=0.495 m, $z$=0.0475 m) and shear (at x=0.495 m, z=0 m) stress components at the mid-span section vs time using mode superposition method. Thin-walled rectangular beam under sinusoidal load. L9 beam model.

for the evaluation of stresses, only the mode superposition is used due to the significant advantage in terms of computational cost and accuracy of results. The convergence analysis, see Fig. 14, for different discretization theories on the cross-section is also provided. Both TE and LE theories are considered. From this figure, it is evident that a low-order theory is sufficient to compute the normal

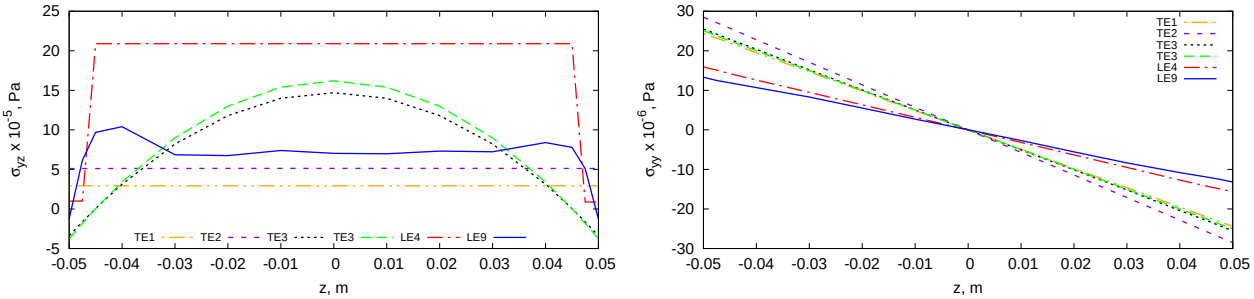


Figure 14: Through-the-thickness stress distribution at the mid-span section and $x$=0.495 m at t= 1.3 s for different LE and TE theories. Thin-walled rectangular beam under sinusoidal load.

stress, whereas a high-order is needed to accurately evaluate the transverse shear stress. For this reason, the LE9 was adopted to perform this analysis. Figure 15 illustrates the axial and shear stress distributions in the thickness direction for different times, including also the comparison with the results obtained using a theory based on linear interpolation (*FSDT-like*).

### 3.3 Two-Stringer spar under sinusoidal loading

As the first typical aeronautical wing structure, a two stringer-spar is considered, see Fig. 16. Free vibration analysis of this structure is reported in [33]. In this paper, the dynamic response through the Newmark method and mode superposition method is performed. The stringers are square for

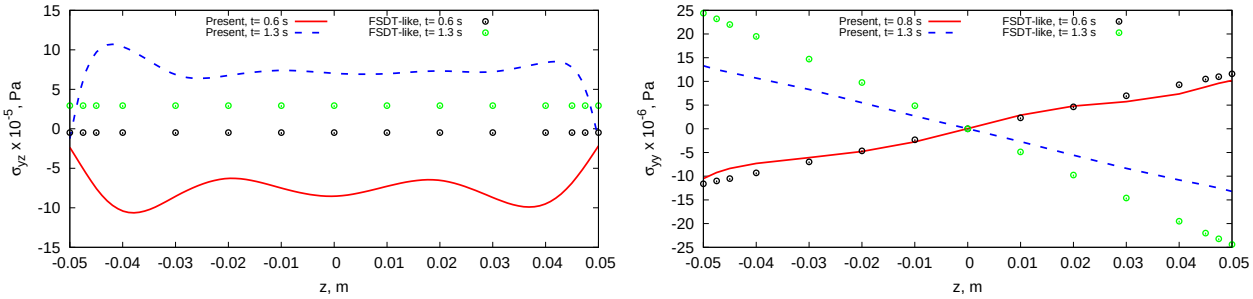


Figure 15: Axial and shear stress components at the mid-span section and $x$=0.495 m vs $z$ at $t$= 0.6 s and $t$= 1.3 s for $\sigma_{yz}$ and at $t$= 0.8 s and $t$= 1.3 s for $\sigma_{yy}$ using mode superposition method (100 modes). Thin-walled rectangular beam under sinusoidal load. L9 beam model vs *FSDT-like*.

convenience; however, as reported by Carrera *et al.* [33], their shape does not affect the validity of the following analysis. This model has the following geometrical data: $L/h$= 3, $A_s$= 0.9×10$^{-3}$ m$^2$, $t$= 1×10$^{-3}$ m. The material properties are: $E$= 75 GPa, $\nu$= 0.33, $\rho$= 2700 kg/m$^3$. The longeron is clamped at $y$=0. The structure is loaded with a single harmonic load applied at a quarter of the

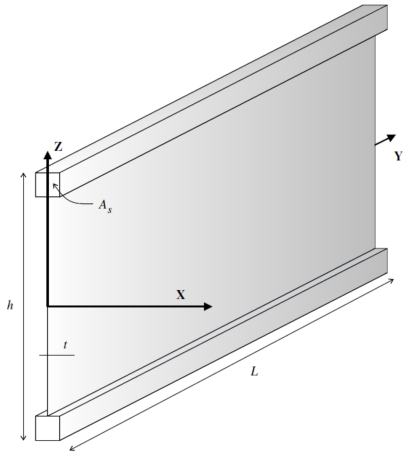


Figure 16: Two-stringer spar.

beam:

$$P_z(t) = P_{z_0} sin(\omega t) \tag{21}$$

where $P_{z_0}$= 1000 N is the amplitude of the sinusoidal load, whereas $\omega$= 7 rad/s is the angular frequency.

For the completeness reasons, the maximum transverse displacement $u_z$ at the load point for different expansion orders using the Newmark method are reported in Table 2. For the following analyses, a L9 beam model is used. Hence, this structure is modelled with 10 B4 finite elements along the $y$-axis and a piece-wise quadratic model on the cross-section (8L9) using the CW methodology. The dynamic response is studied employing the Newmark method, the mode superposition method and

| | $u_z \times 10^5$ [m] | DOFs |
|---|---|---|
| TE 1 | 5.26 | 279 |
| TE 2 | 5.26 | 558 |
| TE 3 | 8.03 | 930 |
| TE 4 | 8.49 | 1395 |
| TE 5 | 9.05 | 1953 |
| TE 10 | 9.35 | 6138 |
| L9 | 9.63 | 4743 |

Table 2: Effect of the different expansion orders on transverse displacement values at the load point of the two-stringers spar under sinusoidal load at $t$= 2 s. Newmark method ($dt$= 0.02 s).

the CUF models over the time interval [0,4] s. The transverse displacement are computed at the mid-span of the structure and in the center of the cross-section. Regarding the Newmark method, a convergence study is made on the $dt$ to be used in the displacement assessment. Figure 17a shows the transverse displacement for a different number of steps. As a result, 200 steps ($dt$= 0.02 s) are sufficient for this type of analysis. On the other hand, Fig. 17b presents the convergence analysis on the number of modes for the mode superposition method. Data in Fig. 17b suggest that 30 modes are sufficient for the following analyses. Finally, the comparison between the two methods for the transverse displacement evaluated in the mid-span is depicted in Fig. 17c. As evident in these

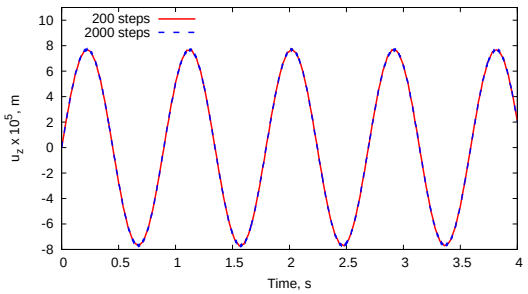


(a) Convergence study on the $dt$ for the Newmark method

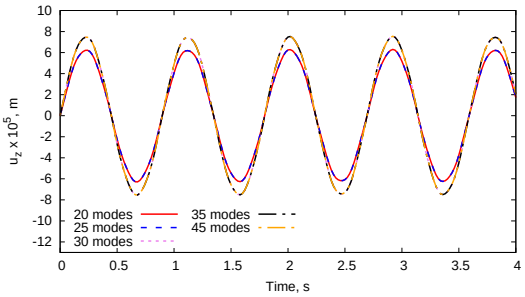


(b) Convergence study on the number of modes for the mode superposition method

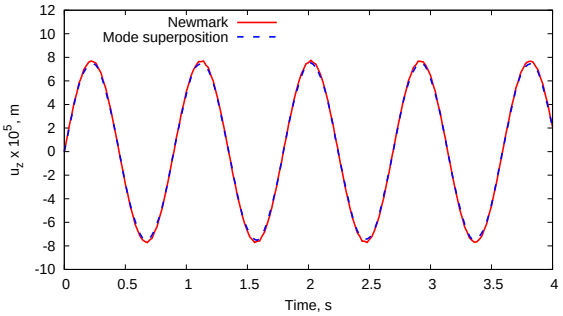


(c) Comparison between the Newmark method ($dt$= 0.02 s) and the mode superposition method (30 modes)

Figure 17: Time-dependent transverse displacement at mid-span. Two-stringer spar under sinusoidal load. L9 beam model.

figures, both methods give good results and with a similar computational cost for the evaluation of displacements. Subsequently, for the same structure, an evaluation of both the axial loads and mean shear flow is reported. In particular, axial loads in the upper stringer and shear flows on panels/webs are evaluated. Using the mode superposition method, a new convergence analysis on the modes is necessary for a correct stress assessment. In particular, for this case, 150 modes are used and also the locking correction (MITC) is activated [42]. Figure 18 shows the distribution of the axial load in the upper stringer, $P$, at $y$= 0, and the mean shear flows in the panel, $q$, at $y = L/4$, with respect to the time. Furthermore, Fig. 19 illustrates the axial and shear stress distributions in the thickness

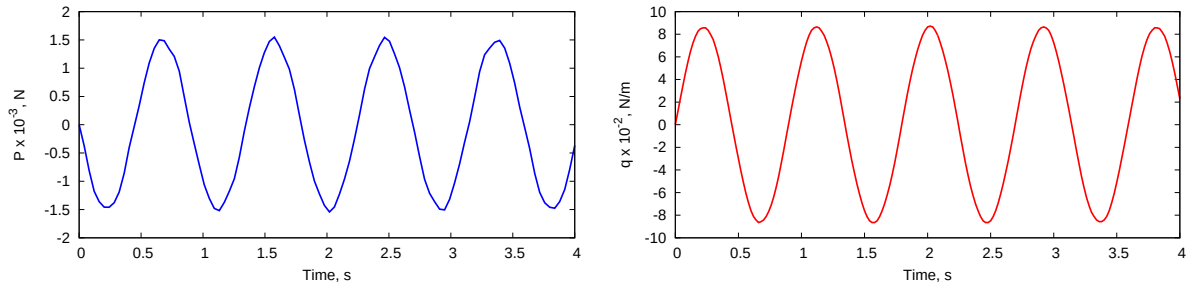


(a) $P$ in the upper stringer at $y$= 0 m (b) $q$ in the panel

Figure 18: Axial load ($P$) and mean shear flows ($q$) versus time. Two-stringers spar under sinusoidal load. Mode superposition method (150 modes). L9 beam model.

direction at $t$= 2 s in comparison with the data obtained using a theory based on linear interpolation (*FSDT-like*). It can be observed that to analyze complex structures, such as thin-walled structures, a low-order theory is not very accurate to evaluate stress distributions.

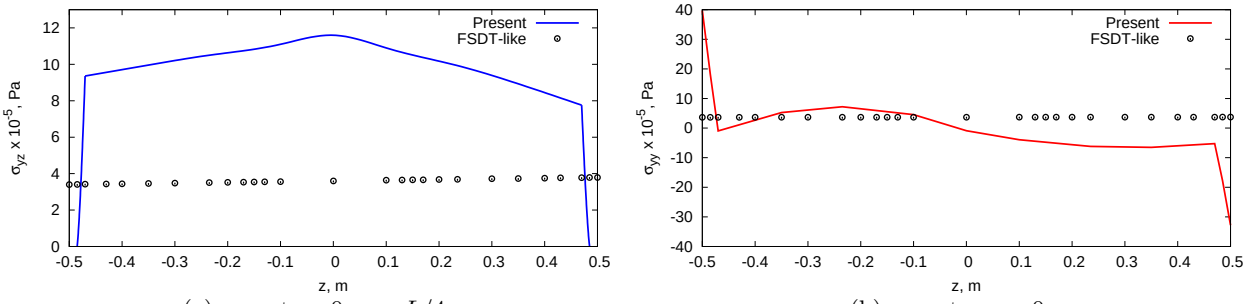


(a) $\sigma_{yz}$ at $x$=0, $y = L/4$ (b) $\sigma_{yy}$ at $x$=$y$=0

Figure 19: Axial and shear stress components in the thickness direction at $t$= 2 s using mode superposition method (150 modes). Two-stringer spar under sinusoidal load. L9 beam model.

The following considerations arise:

- The CW models are used because of the accurate evaluation of the solution. Both global and local modes are correctly obtained with a significant reduction of the computational costs;

- Both the Newmark method and mode superposition method achieve a good evaluation of the transverse displacements with a similar computational cost;
- For a correct evaluation of the stresses, the mode superposition method was preferred to the Newmark method due to the correct calculation of the modes through the CW approach, but also for the considerable computational savings if complex structures are analyzed.

### 3.4 Wing box under sinusoidal loading

The dynamic response of a cantilever wing box is studied in the following case. The model has the following dimensions: $L$= 3 m, $b$= 1 m, $h$= 0.5 m. The thickness of the panels is $t$= $2\times10^{-3}$ m. The spar caps area is $A_s$= $1.6\times10^{-3}$ m$^2$. The structure is made of an aluminium with the following data: $E$= 75 GPa, $\nu$= 0.33 and $\rho$= 2770 kg/m$^3$. The wing box is reported in Fig. 20, where it is also possible to see the load point application. The structure is modelled with 10 B4 finite elements along

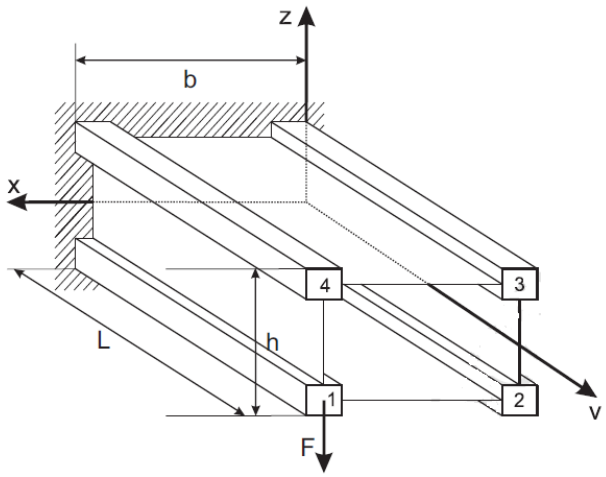


Figure 20: Wing box model.

the $y$-axis and a piece-wise quadratic approximation on the cross-section (8L9). In the stringer 1 and at $y = L$, it is applied a sinusoidal load having amplitude $P_0$= 10000 N and angular frequency $\omega$= 3 rad/s. First, time-dependent transverse displacements at the load application point are shown in Fig. 21 for different theories using the Newmark method. Table 3 provides the maximum displacement at the center of the stringer 1 for different theories. From these data, it appears that LE is a good choice to adopt for the following analysis. As in previous cases, for this type of structure, the CW approach discretization is used. Performing a convergence study for both the Newmark method ($dt$) and mode superposition method (number of modes) is necessary for a correct realization of the analyses. Figures 22a and 22b provide the convergence analysis for choosing the correct ($dt$) and

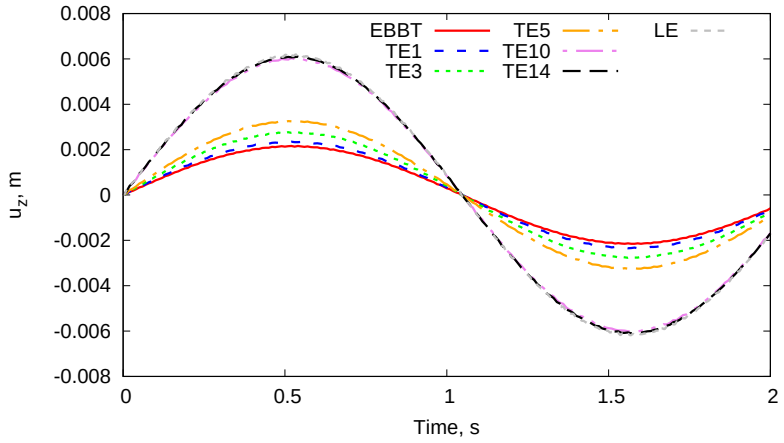


Figure 21: Time-dependent transverse displacement at the load application point with Newmark method ($dt$= 0.01 s) for different theories. Wing box under sinusoidal load.

| Theory | Stringer 1 |
|---|---|
| - | $u_{z_{max}}$ [mm] |
| EBBT | 2.17 |
| TE 1 | 2.36 |
| TE 3 | 2.78 |
| TE 5 | 3.28 |
| TE 10 | 6.07 |
| TE 14 | 6.11 |
| L9 | 6.19 |

Table 3: Maximum transverse displacement at the center of the stringer 1 obtained using different theories at $t$= 0.5 s with the Newmark method. Wing box model.

the number of modes to use in the subsequent displacement evaluations. The comparison between the Newmark method and the mode superposition method and reference results [29] is reported in Fig. 22c. Subsequently, an evaluation of the stress distributions and also of both the axial load and

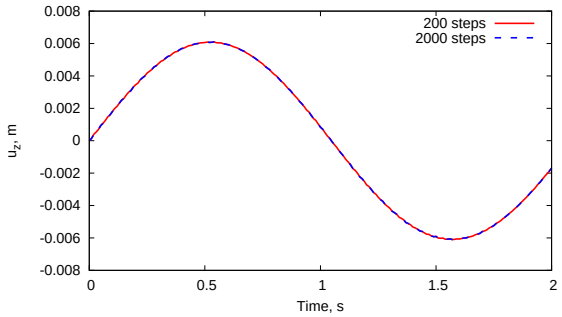


(a) Convergence study on the $dt$ for the Newmark method

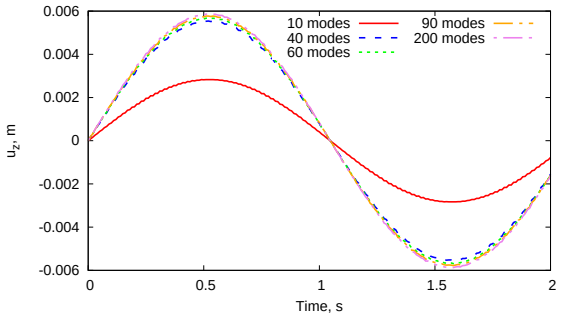


(b) Convergence study on the number of modes for the mode superposition method

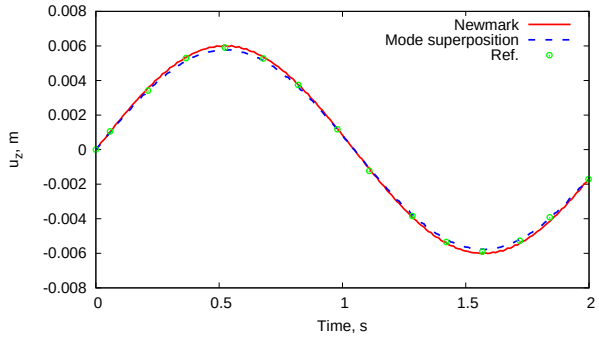


(c) Comparison between mode superposition (90 modes) and Newmark method ($dt$= 0.01 s) and Ref. [29]

Figure 22: Time-dependent transverse displacement at the load application point. Wing box under sinusoidal load. L9 beam model.

mean shear flow is reported. This analysis requires a more refined model, and for this case, after a convergence analysis, we have chosen to adopt 52L9. A convergence analysis on the number of modes for the stress evaluation is carried out, and 150 modes are considered in the following analysis. Figure 23 depicts the distribution of the axial load in the upper stringer, $P$, at $y$= 0, and the mean shear flows in the panel, $q$, at $y = L/4$, as a function of the time. Furthermore, axial and shear stress distributions in the thickness direction for different times are depicted in Fig. 24, showing the difference with the results obtained using a theory based on linear interpolation (*FSDT-like*).

### 3.5 Three-bay wing under gust loading

As a final example, the gust response of a cantilever aircraft wing is addressed. The NACA 2415 airfoil with two spar webs and four spar caps is used. This airfoil, showed in Fig. 25, has the following characteristics: chord $c$= 1 m, length $L$= 6 m, thickness of each panel is equal to $3 \times 10^{-3}$

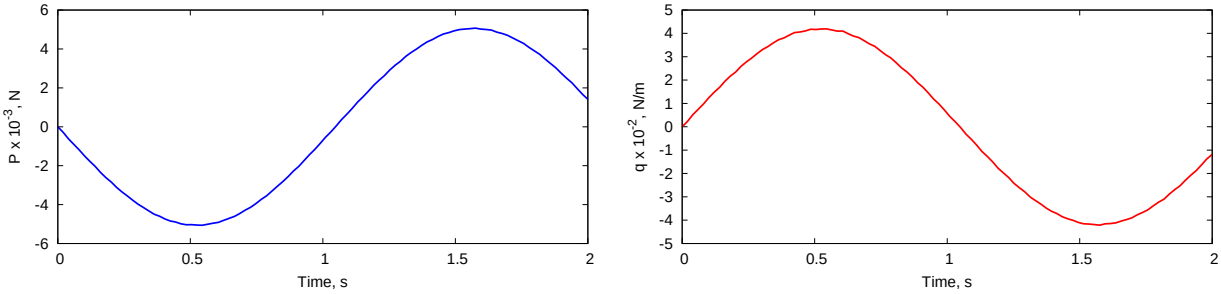


(a) $P$ in the upper stringer at $y$= 0 m (b) $q$ in the panel, at $y$= 0.9 m

Figure 23: Axial load ($P$) and mean shear flows ($q$) versus time. Wing box under sinusoidal load. Mode superposition method (150 modes). L9 beam model.

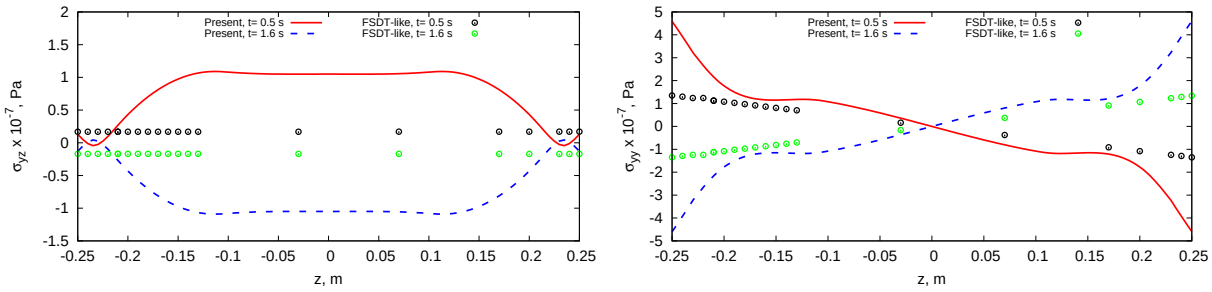


(a) $\sigma_{yz}$ at $x$=0.96 m, $y = L/2$ (b) $\sigma_{yy}$ at $x$=0.96 m, $y$=0

Figure 24: Axial and shear stress components in the thickness direction using the mode superposition method (150 modes). Wing box under sinusoidal load. L9 beam model.

m and thickness of the spar webs is $5 \times 10^{-3}$ m. The dimensions of the flanges of the longerons are reported in [33]. The whole structure is made of isotropic material. The material properties are: $E$= 75 GPa, $\nu$= 0.33, $\rho = 2700$ kg/m$^3$. This structure is modelled with 9 B4 finite elements along

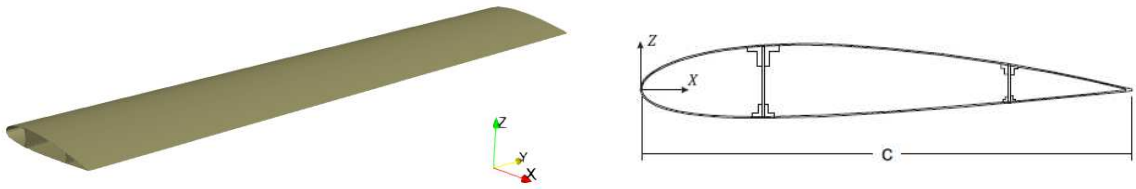


Figure 25: The complete NACA wing.

the $y$-axis and a piece-wise quadratic model on the cross-section (49L9) using the CW approach. Readers are referred to [43] for the free vibration analysis of this wing structure. Here, the discrete one-minus-cosine response of the NACA wing is considered. The airplane with a wing loading $W/S$= 378.6 kg/m$^2$ is supposed to fly at sea level ($\rho_\infty = 1.225$ kg/m$^3$) with velocity $V_\infty = 80$ m/s. At 1-g flight condition, a vertical gust with intensity $U_0 = 10$ m/s and duration $t_g = 0.4$ s is considered. A $CL_\alpha = 7.6$ rad$^{-1}$ was calculated by means of XFLR5 [44] and XFoil [45] programs and by supposing

inviscid flow. Both mode superposition method and Newmark method are used to perform gust response analysis. Figures 26a and 26b provide the convergence analysis for choosing the correct ($dt$) and the number of modes to use in the subsequent displacement evaluations. The comparison between the Newmark method and the mode superposition method is reported in Fig. 26c. After

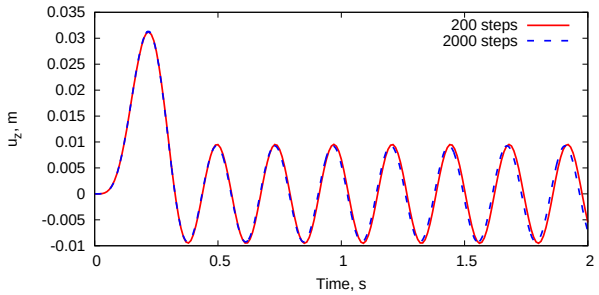


(a) Convergence study on the $dt$ for the Newmark method

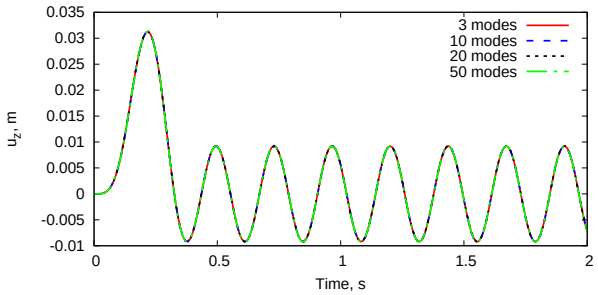


(b) Convergence study on the number of modes for the mode superposition method

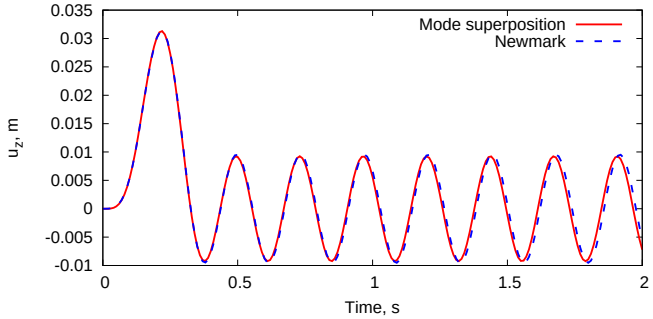


(c) Comparison between mode superposition (3 modes) and Newmark method ($dt$= 0.01 s)

Figure 26: Time-dependent transverse displacement at the wing tip subjected to gust load.

the convergence analysis, it turns out that only 3 modes are needed to compute the transverse displacement using the mode superposition, instead, at least 200 steps are needed adopting the Newmark method. Regarding stress analysis, another convergence analysis is needed. As a result, 15 modes have to be used to accurately evaluate stress distributions with the mode superposition method. Figure 27 reports the transverse stress component, $\sigma_{yz}$, with respect to the time. Moreover, Fig. 28 illustrates the axial and shear stress distributions in the thickness direction at $x$= 0.25 m, $y$= L/2 and $t$= 0.2 in comparison with the data obtained using a theory based on linear interpolation (*FSDT-like*). Results suggest the impossibility of accurately evaluating stresses adopting a low-order theory.

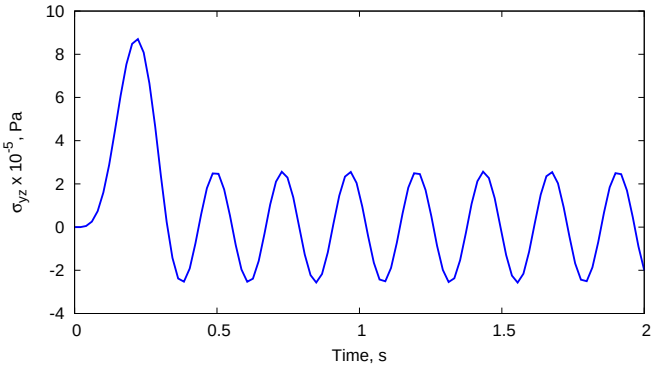


Figure 27: Transverse stress component, $\sigma_{yz}$, in $x$=0.25 m, $y$= L/2 and $z$= 0.02 of the NACA wing under gust load versus time. Mode superposition method using 15 modes.

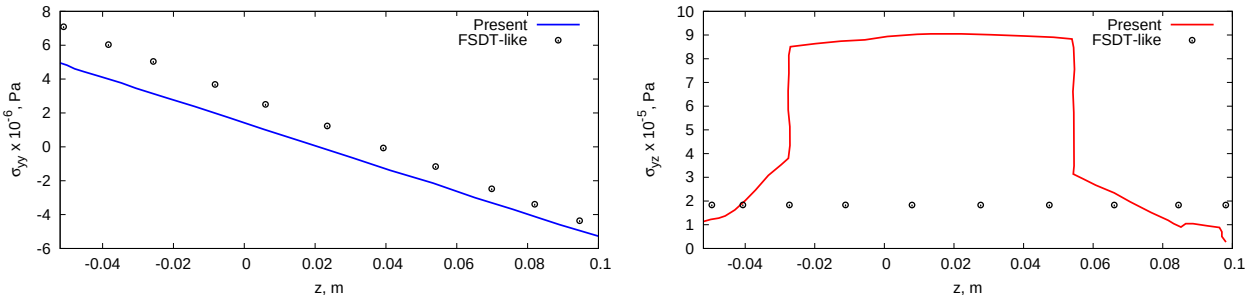


Figure 28: Through-the-thickness distribution of the axial, $\sigma_{yy}$, and transverse, $\sigma_{yz}$, stress in $x$=0.25 m and $y$= L/2 at $t$= 0.2 s of the NACA wing subjected to gust load. Mode superposition (15 modes).

## 4 Conclusions

In this article, the dynamic response analysis of typical aerospace structures has been investigated through refined and component-wise models in conjunction with two different dynamic resolution techniques, namely the Newmark method and the mode superposition method. As general guidelines and recommendations, it can be stated that both methods can be used for the evaluation of displacements with a comparable level of accuracy and computational cost. In contrast, because CUF-based models are able to detect accurately low- to high-frequency modes, mode superposition may be used successfully for the evaluation of stresses, eventually even in a more efficient manner.

## References

[1] S. Hernandez, E. Menga, P. Naveira, C. Lopez, A. Baldomir, M. Cid, S. Moledo, and D. Freire. Dynamic analysis of assembled aircraft structures with nonlinear joints. In *58th AIAA/ASCE/AHS/ASC Structures, Structural Dynamics, and Materials Conference*, page 1592, 2017.

[2] E. Carrera, M. Filippi, and E. Zappino. Free vibration analysis of rotating composite blades via carrera unified formulation. *Composite Structures*, 106:317–325, 2013.

[3] D.E. Beskos and K.L. Leung. Dynamic response of plate systems by combining finite differences, finite elements and laplace transform. *Computers & Structures*, 19(5-6):763–775, 1984.

[4] L. Librescu and J. Oh, S.Y.and Hohe. Dynamic response of anisotropic sandwich flat panels to underwater and in-air explosions. *International Journal of Solids and Structures*, 43(13):3794–3816, 2006.

[5] P.K. Parhi, S.K. Bhattacharyya, and P.K. Sinha. Dynamic analysis of multiple delaminated composite twisted plates. *Aircraft Engineering and Aerospace Technology*, 71(5):451–461, 1999.

[6] P. Mata, S. Oller, and A.H. Barbat. Dynamic analysis of beam structures considering geometric and constitutive nonlinearity. *Computer Methods in Applied Mechanics and Engineering*, 197(6-8):857–878, 2008.

[7] J.A. Main, R.A. Carlin, E. Garcia, S.W. Peterson, and A.M. Strauss. Dynamic analysis of space-based inflated beam structures. *The Journal of the Acoustical Society of America*, 97(2):1035–1045, 1995.

[8] L. Euler. De curvis elasticis. Geneva, 1774.

[9] S.P. Timoshenko. On the corrections for shear of the differential equation for transverse vibration of prismatic bars. *Philosophical Magazine*, 41:744–746, 1922.

[10] S.P. Timoshenko. On the transverse vibrations of bars pf uniform cross section. *Philosophical Magazine*, 41:122–131, 1922.

[11] F. Gruttmann and W. Wagner. Shear correction factors in timoshenko's beam theory for arbitrary shaped cross-sections. *Computational Mechanics*, 27(3):199–207, 2001.

[12] W. Carnegie and J. Thomas. The effects of shear deformation and rotary inertia on the lateral frequencies of cantilever beams in bending. *Journal of Engineering for Industry*, 94(1):267–278, 1972.

[13] M. Levinson. A new rectangular beam theory. *Journal of Sound and Vibration*, 74(1):81–87, 1981.

[14] E. Carrera, A. Pagani, M. Petrolo, and E. Zappino. Recent developments on refined theories for beams with applications. *Mechanical Engineering Reviews*, 2(2):14–00298, 2015.

[15] E. Carrera, M. Cinefra, M. Petrolo, and E. Zappino. *Finite element analysis of structures through unified formulation*. John Wiley & Sons, 2014.

[16] E. Carrera. Theories and finite elements for multilayered, anisotropic, composite plates and shells. *Archives of Computational Methods in Engineering*, 9(2):87–140, 2002.

[17] E. Carrera. Theories and finite elements for multilayered plates and shells: a unified compact formulation with numerical assessment and benchmarking. *Archives of Computational Methods in Engineering*, 10(3):215–296, 2003.

[18] E. Carrera, G. Giunta, and M. Petrolo. *Beam structures: classical and advanced theories*. John Wiley & Sons, 2011.

[19] E. Carrera and G. Giunta. Refined beam theories based on a unified formulation. *International Journal of Applied Mechanics*, 2(01):117–143, 2010.

[20] E. Carrera and A. Varello. Dynamic response of thin-walled structures by variable kinematic one-dimensional models. *Journal of Sound and Vibration*, 331(24):5268–5282, 2012.

[21] E. Carrera and M. Petrolo. Refined beam elements with only displacement variables and plate/shell capabilities. *Meccanica*, 47(3):537–556, 2012.

[22] K.J. Bathe. *Finite element procedures*. Klaus-Jurgen Bathe, 2006.

[23] R.W. Clough and J. Penzien. *Dynamics of Structures*. 2nd York, 1992.

[24] A.B. Chaudhary and K.J. Bathe. A solution method for static and dynamic analysis of three-dimensional contact problems with friction. *Computers & Structures*, 24(6):855–873, 1986.

[25] G. Borino and G. Muscolino. Mode-superposition methods in dynamic analysis of classically and non-classically damped linear systems. *Earthquake Engineering & Structural Dynamics*, 14(5):705–717, 1986.

[26] A.M. Claret and F. Venancio-Filho. A modal superposition pseudo-force method for dynamic analysis of structural systems with non-proportional damping. *Earthquake Engineering & Structural Dynamics*, 20(4):303–315, 1991.

[27] O.E. Hansteen and K. Bell. On the accuracy of mode superposition analysis in structural dynamics. *Earthquake Engineering & Structural Dynamics*, 7(5):405–411, 1979.

[28] Z.D. Ma and I. Hagiwara. Improved mode-superposition technique for modal frequency response analysis of coupled acoustic-structural systems. *AIAA Journal*, 29(10):1720–1726, 1991.

[29] A. Pagani, M. Petrolo, G. Colonna, and E. Carrera. Dynamic response of aerospace structures by means of refined beam theories. *Aerospace Science and Technology*, 46:360–373, 2015.

[30] N.R. Maddox. On the number of modes necessary for accurate response and resulting forces in dynamic analyses. *Journal of Applied Mechanics*, 42:516, 1975.

[31] R.R. Craig and A.J. Kurdila. *Fundamentals of structural dynamics*. John Wiley & Sons, 2006.

[32] E.F. Bruhn. Analysis and design of flight vehicle structures. *SR Jacobs & Associates, Inc., USA*, 1973.

[33] E. Carrera, A. Pagani, and M. Petrolo. Component-wise method applied to vibration of wing structures. *Journal of Applied Mechanics*, 80(4):041012, 2013.

[34] E. Carrera and A. Pagani. Free vibration analysis of civil engineering structures by component-wise models. *Journal of Sound and Vibration*, 333(19):4597–4620, 2014.

[35] E. Carrera, M. Maiarú, and M. Petrolo. Component-wise analysis of laminated anisotropic composites. *International Journal of Solids and Structures*, 49(13):1839–1851, 2012.

[36] E. Carrera, A. Pagani, and M. Petrolo. Classical, refined, and component-wise analysis of reinforced-shell wing structures. *AIAA Journal*, 51(5):1255–1268, 2013.

[37] E. Carrera and A. Pagani. Multi-line enhanced beam model for the analysis of laminated composite structures. *Composites Part B: Engineering*, 57:112–119, 2014.

[38] E. Carrera and A. Pagani. Analysis of reinforced and thin-walled structures by multi-line refined 1D/beam models. *International Journal of Mechanical Sciences*, 75:278–287, 2013.

[39] E. Carrera, G. Giunta, P. Nali, and M. Petrolo. Refined beam elements with arbitrary cross-section geometries. *Computers & Structures*, 88(5-6):283–293, 2010.

[40] E. Carrera, M. Petrolo, and P. Nali. Unified formulation applied to free vibrations finite element analysis of beams with arbitrary section. *Shock and Vibration*, 18(3):485–502, 2011.

[41] MSC Nastran. Dynamic analysis user's guide. *MSC Software*, 2010.

[42] E. Carrera, A.G. de Miguel, and A. Pagani. Extension of MITC to higher-order beam models and shear locking analysis for compact, thin-walled, and composite structures. *International Journal for Numerical Methods in Engineering*, 112(13):1889–1908, 2017.

[43] A. Pagani. *Component-wise models for static, dynamic and aeroelastic analyses of metallic and composite aerospace structures.* PhD thesis, Ph.D Thesis, 2015.

[44] A. Deperrois. *XFLR5, 2003-2015.* url : http://www.xflr5.com/xflr5.htm.

[45] M. Drela. XFOIL: An analysis and design system for low Reynolds number airfoils. In *Low Reynolds Number Aerodynamics*, pages 1–12. Springer, 1989.